

 Open access • Journal Article • DOI:10.1103/PHYSREVB.72.214102

Improved long-range reactive bond-order potential for carbon. I. Construction

— [Source link](#) 

Jan H. Los, Luca M. Ghiringhelli, Evert Jan Meijer, Annalisa Fasolino ...+1 more authors





Institutions: Radboud University Nijmegen, University of Amsterdam

Published on: 02 Dec 2005 - Physical Review B (American Physical Society)

Topics: Ab initio, Bond order, Triple bond, Ab initio quantum chemistry methods and Bond length

Related papers:

- [Intrinsic ripples in graphene](#)
- [Intrinsic long-range bond-order potential for carbon: Performance in Monte Carlo simulations of graphitization](#)
- [A reactive potential for hydrocarbons with intermolecular interactions](#)
- [Electric Field Effect in Atomically Thin Carbon Films](#)
- [Finite temperature lattice properties of graphene beyond the quasiharmonic approximation.](#)

Share this paper:    

View more about this paper here: <https://typeset.io/papers/improved-long-range-reactive-bond-order-potential-for-carbon-8g4cu7ok0o>

PDF hosted at the Radboud Repository of the Radboud University Nijmegen

The following full text is a publisher's version.

For additional information about this publication click this link.

<http://hdl.handle.net/2066/32617>

Please be advised that this information was generated on 2022-05-30 and may be subject to change.

Improved long-range reactive bond-order potential for carbon. I. ConstructionJan H. Los,¹ Luca M. Ghiringhelli,² Evert Jan Meijer,² and A. Fasolino^{1,2}¹*IMM, Radboud University Nijmegen, Toernooiveld 1, 6525 ED Nijmegen, The Netherlands*²*van't Hoff Institute for Molecular Sciences, Universiteit van Amsterdam, Nieuwe Achtergracht 166, 1018 WV Amsterdam, The Netherlands*

(Received 15 July 2005; published 2 December 2005)

We present LCBOPII, an improvement of the long-range carbon bond-order potential (LCBOP) by Los and Fasolino [Phys. Rev. B **68**, 024107 (2003)]. LCBOPII contains a coordination dependent medium range term for bond distances between 1.7 and 4 Å, meant to reproduce the dissociation energy curves for single, double, and triple bonds and improve the reactive properties as well as the description of the liquid and of low coordinated phases. Other features of LCBOPII are a coordination dependent angular correlation, a correction for antibonding states, and a conjugation dependent torsional interaction based on *ab initio* calculations of the torsional barriers for a set of molecular configurations. We present results for the geometry and energetics of the graphite-to-diamond transformation and of the vacancy in diamond and graphite as well as the prediction of the energy barrier of the 5-77-5 defect in graphite and graphene for which *ab initio* results are available only for unsuitably small samples. In the accompanying paper (Ghiringhelli *et al.*, Phys. Rev. B **72**, 214103 (2005)) we use LCBOPII to evaluate several properties, including the equation of state, of liquid carbon.

DOI: 10.1103/PhysRevB.72.214102

PACS number(s): 81.05.Uw, 34.20.Cf, 67.80.Mg

I. INTRODUCTION

The construction of accurate, reactive, and computationally efficient potentials describing the atomic interactions in covalent materials is still a challenge. Reactive potentials, that allow coordination changes, are of great interest for studying structural properties and phase transformation of these materials in classical, large scale simulations, where density functional (DF) and even tight-binding methods become computationally too intensive. Many good nonreactive (i.e., not permitting coordination changes) potentials or force fields exist for several materials¹ for near-equilibrium structures. One of the first reactive potentials was developed by Finnis and Sinclair for highly coordinated, metallic systems.² Their approach, now known as the embedded atom method (EAM) was adopted later by other authors who applied it also to covalent materials.^{3,4} Soon after the appearance of the EAM, Stillinger and Weber (SW) proposed a simple and elegant reactive potential for silicon,⁵ which was refined and improved later by others^{6,7} and also applied to carbon.⁸ The difference between the EAM and the SW approach lies in the fact that, in the original EAM, many body correlations depend mainly on coordination number, whereas in the SW potential they depend explicitly on bond angles. An important new contribution to the evolution of reactive potentials for covalent materials was made by Tersoff, who introduced a so-called bond-order potential (BOP) for silicon,^{9–11} which was parametrized later also for carbon.¹² A BOP contains a built-in correlation between coordination and bond strength, the so-called bond order. This term, expressed through a bond angle dependent term, is fitted to the binding energies of a series of bulk lattices from low to high coordinated ones, and yields a more or less smooth and natural interpolation between the different coordination states.

Nowadays there exist also reactive potentials that resemble the nonreactive force field potentials, such as the ReaxFF potentials.^{13,14} In these models the total energy is the

sum of various more or less independent contributions.

Carbon represents a new challenge for constructing empirical potentials. Due to its small dimension, π -bonding between undercoordinated atoms is particularly efficient for carbon. In contrast to silicon, carbon structures exhibit strong double and triple bonds, and also strong fractional bonding states, like in graphite where the covalent intraplanar bonds, often denoted as 4/3 bonds, consist of a σ -bond plus a fraction of a π -bond. In spite of the “undercoordination” graphite is even slightly more stable than diamond at ambient conditions.

The first BOP including conjugation effects was designed for hydrocarbons by Brenner,¹⁵ who gave two parametrizations, I and II, the first one giving the best bond distances and the second one giving a better fit of the force constants. Later Brenner published the REBO (reactive bond order) potential,¹⁶ which combines the qualities of Brenner I and Brenner II, and also includes torsional interactions and a correction of the angular correlation for small angles at low coordinations improving the description of small clusters. So far the Brenner potentials, with a cutoff for interatomic interactions of only 2 Å, did not include the long-range (LR) interactions, responsible, e.g., for the interplanar binding in graphite. Although this is of course a very favorable property from a computational point of view, the LR attraction plays a crucial role in many carbon based structures (graphite, intermolecular binding, etc.). Several schemes have been proposed to include LR interactions,^{17–21} the main difficulty being to avoid spoiling the nicely fitted properties of Brenner’s potentials. In view of the shortcomings of all these attempts, giving rise to loss of accuracy and unrealistic interactions, we found that the best solution for this problem was to include LR interactions and reparametrize the short-range (SR) potential, refitting all the bonding properties, including conjugation. This approach has led to a long-range carbon bond-order potential (LCBOP),²² a potential for pure carbon, here denoted as LCBOP I from now on.

An important motivation for the construction of LCBOP1 was to obtain a potential that describes both the liquid and the various solid phases, first of all graphite and diamond, as accurately as possible, making it a suitable tool for realistic, quantitative studies of the phase behavior and phase transitions by employing modern simulation techniques. In a preliminary study of the liquid phase according to LCBOP1,²³ restricted to one temperature (6000 K), we extended LCBOP1 with torsional interactions and a correction of the small angle correlation for low coordinations. This extended LCBOP1, hereafter denoted as LCBOP1⁺, is described in Appendix A. Torsional interactions were added because they had been found to play an important role for the structural properties of the liquid phase, being responsible for a liquid-liquid phase transition (LLPT)²⁴ in simulations with the Brenner II BOP extended with torsional interactions. We have recently used LCBOP1⁺ also for the determination of the liquid-graphite-diamond phase diagram of carbon up to extreme temperatures and pressures.²⁵

Both the results for the liquid phase and the phase diagram, so far based on LCBOP1⁺, show a promising agreement with available data from density functional molecular dynamics (DFMD)²⁶ simulations and experimental data. For example, with LCBOP1⁺ no LLPT was found in agreement with DFMD, most likely due to weaker torsional interactions for conjugated bonds as compared to the extended Brenner II BOP. For LCBOP1⁺ these interactions were fitted to recent *ab initio* calculations²⁷ of the torsional barrier for such bonds. The pressure-volume isotherms at 6000 K from DFMD simulations are reasonably well reproduced by LCBOP1⁺ as well as the trend in the coordination statistics over a wide range of densities, in contrast to Brenner's BOP's without LR interactions.

However, significant differences in the radial distribution function (rdf) for the liquid phase between DFMD and LCBOP1⁺ prompt one to further improvement of the potential. Although the positions of the extrema in the rdfs at various densities are reproduced reasonably well, the minima and maxima according to LCBOP1⁺ are clearly more pronounced than those according to DFMD.²³ In particular, LCBOP1⁺, and also Brenner's BOPs, give rise to a very deep minimum around the cutoff range for the short-range interactions. It is tempting to assign this effect to the strong gradients within the cutoff range, an artifact of the cutoff. In order to shine more light on this point, we performed *ab initio* calculations of the dissociation energy curve for a single bond, as described in Appendix B, and compared it to those according to LCBOP1⁺ and REBO. The comparison is shown in Fig. 1. Clearly, with a SR cutoff radius of 2.2 Å (2.0 Å for REBO) LCBOP1⁺ cannot reproduce the energy of -2 eV at 2.2 Å in the single bond dissociation found in the DFMD calculation. Note that beyond the SR cutoff radius there are only LR interactions between the two dissociating fragments, which give rise to an effective repulsion between the fragments in the range from 2.2 to 3.5 Å. For REBO the interaction between the fragments beyond 2 Å vanishes altogether. In this case, we may certainly assume that the *ab initio* results are more reliable, and obviously this discrepancy could very well be the reason for the mentioned difference in the liquid structure.

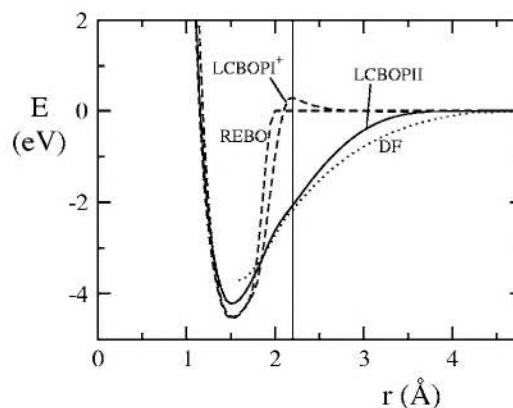


FIG. 1. Bonding energy for the single bond in $(\text{CH}_3)_3\text{C}-\text{C}(\text{CH}_3)_3$ as a function of the central C-C distance, calculated by DF (dotted line), by LCBOP2 (solid line), and by REBO and LCBOP1⁺ (dashed lines).

The above discrepancy inspired us to further improvements of LCBOP1⁺. The resulting potential is denoted LCBOP2. The many modifications and improvements of LCBOP2, as compared LCBOP1⁺, require a complete description, which is given in Sec. II. LCBOP2 reproduces much better the dissociation energy curves for single, double, and triple bonds by the addition of attractive interactions between atoms at middle range (MR) distances between 1.7 and 4 Å. These MR interactions, which extend the covalent bonding where this is appropriate, depend on the mutual reactivity between atoms, which is quantified in terms of the bond angles and of the presence of dangling bonds, as described in Sec. II D. Further improvements of LCBOP2 include (i) an extended and more dynamic coordination dependence of the angular correlation, (ii) a correction for antibonding states by the addition of a new term to the bond order, (iii) an extended conjugation dependence of the torsional interactions based on *ab initio* calculations of the torsional barriers for a set of molecular configurations, (iv) a different definition of the torsion angle not producing spurious torsion, and (v) a more natural interpolation approach for noninteger coordination states.

After the description of LCBOP2 in Sec. II, structural and elastic properties for solid phase structures, including the diamond (111) and (100) reconstructed surfaces, will be presented and discussed in Sec. III. In this section we present also results concerning the geometry and energetics of the diamond to graphite transformation and of the vacancy in graphite and diamond as well as the prediction of LCBOP2 for the energy barrier for the formation of the so-called 5-7-5 defect. In Appendix A, we describe the previous version of the potential LCBOP1⁺ and in Appendix B, we give details of the DF calculations used to develop LCBOP2. In the companion paper,²⁸ the results of an extended study of liquid carbon according to LCBOP2 are given, covering a large pressure-temperature domain of the phase diagram, and are compared to *ab initio* data, where available.

II. LCBOP2

For LCBOP2, the total binding energy E_b for a system consisting of N_{at} is given by

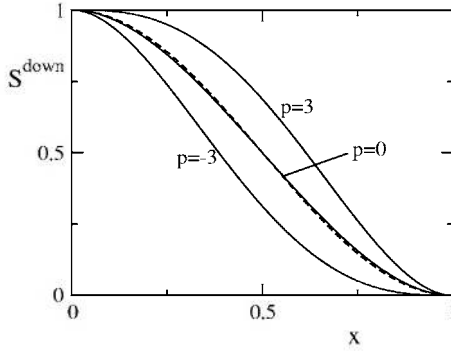


FIG. 2. Switch function $S^{\text{down}}(x)$ for $p = -3, 0, 3$ (solid lines) compared to the Brenner's cutoff function $f_{ij} = 1/2[1 + \cos(\pi x)]$ Ref. 15 (dashed line).

$$E_b = \frac{1}{2} \sum_{i,j}^{N_{at}} \left(S_{sr,ij}^{\text{down}} V_{ij}^{sr} + S_{sr,ij}^{\text{up}} V_{ij}^{lr} + \frac{1}{Z_i^{\text{mr}}} S_{mr,ij}^{\text{up}} V_{ij}^{\text{mr}} \right), \quad (1)$$

where $V_{ij}^{sr} = V^{sr}(r_{ij})$ describes the covalent, short-range interactions, $V_{ij}^{lr} = V^{lr}(r_{ij})$ accounts for the long-range nonbonded interactions, and $V_{ij}^{\text{mr}} = V^{\text{mr}}(r_{ij})$ represents the remainder of bonded (attractive) interactions between atoms at middle-range distances. Here $r_{ij} = |\mathbf{r}_i - \mathbf{r}_j|$ is the interatomic distance. The middle-range attractive interaction, not present in LCBOP, is inspired and based on the *ab initio* calculations of the dissociation energy curves for single, double, and triple bonds (see Appendix B). The prefactor $1/Z_i^{\text{mr}}$, where Z_i^{mr} is an effective middle-range coordination number defined in Sec. II D, takes into account many body effects. The switch functions $S_{sr,ij}^{\text{down}} = S_{sr}^{\text{down}}(r_{ij})$, $S_{sr,ij}^{\text{up}} = S_{sr}^{\text{up}}(r_{ij})$, and $S_{mr,ij}^{\text{up}} = S_{mr}^{\text{up}}(r_{ij})$, described in detail in Sec. II A provide a smooth connection between the various interaction contributions.

A. Switch functions

In the description of LCBOP, we will make use of two families of switch functions, $S^{\text{down}}(x)$ and $S^{\text{up}}(x)$, being defined as

$$S^{\text{down}}(x) = \Theta(-x) + \Theta(x)\Theta(1-x)(1+2x+px^2)(1-x)^2 \quad (2)$$

and

$$S^{\text{up}}(x) = 1 - S^{\text{down}}(x) \quad (3)$$

respectively, where $\Theta(x)$ is the heavyside step function. As shown in Fig. 2, the parameter p , ranging in the interval $[-3, 3]$, offers a certain freedom in the choice of the shape of the switch function while staying monotonic within $x \in [0, 1]$. To realize a switch as a function of a given quantity q (e.g., distance or coordination) within a desired interval $[q_{\min}, q_{\max}]$ the dimensionless argument x is defined as

$$x = x(q) = \frac{q - q_{\min}}{q_{\max} - q_{\min}}. \quad (4)$$

In the description of the LCBOP, each switch function,

labeled by an appropriate subscript, is specified by the three numbers q_{\min} , q_{\max} , and p , which are given in Table I.

B. Short-range potential V^{sr}

The potential V_{ij}^{sr} is a Brenner type of bond-order potential similar to that of LCBOP, but with several important modifications. It reads:

$$V_{ij}^{sr} = V_{R,ij}^{sr} - B_{ij} V_{A,ij}^{sr} \quad (5)$$

where V_R^{sr} and V_A^{sr} are repulsive and attractive radial pair potentials given by

$$V_R^{sr}(r) = A^{sr} \exp(-\alpha r), \quad (6)$$

$$V_A^{sr}(r) = B_1^{sr} \exp(-\beta_1 r) + B_2^{sr} \exp(-\beta_2 r). \quad (7)$$

The bond order B_{ij} includes the many body effects and is the sum of several terms:

$$B_{ij} = \frac{1}{2}(b_{ij} + b_{ji}) + F_{ij}^{\text{conj}} + A_{ij} + T_{ij}, \quad (8)$$

where b_{ij} depends on the bond angles and F_{ij}^{conj} accounts for conjugation. With respect to LCBOP we have added the terms A_{ij} and T_{ij} , which account for the effects of the presence of occupied antibonding states and of torsion, respectively.

1. Term b_{ij}

The bond angle dependent part b_{ij} is given by

$$b_{ij} = \left(1 + \sum_{k \neq i,j} S_N^{\text{down}}(r_{ik}) H(\delta r_{ijk}) G(\cos \theta_{ijk}, N_{ijk}) \right)^{-1/2} \quad (9)$$

where the summation runs over all neighbors k ($\neq j$) of i , θ_{ijk} is the bond angle between the bonds ij and ik , and $\delta r_{ijk} = r_{ij} - r_{ik}$. The reduced coordination number N_{ijk} is defined as

$$N_{ijk} = \sum_{l \neq i,j,k} S_{N,il}^{\text{down}} = N_i - S_{N,ij}^{\text{down}} - S_{N,ik}^{\text{down}}, \quad (10)$$

where N_i is the coordination of atom i defined as

$$N_i = \sum_{j \neq i} S_{N,ij}^{\text{down}} \quad (11)$$

and $S_{N,ij}^{\text{down}} = S_N^{\text{down}}(r_{ij})$. As compared to the LCBOP, we have modified the angular function G , making it coordination dependent in order to improve the energetics of configurations with small bond angles. Such a correction of the angular correlation for small angles was also included in the REBO potential, switching from the maximal to a weaker angular correlation for coordinations from 3.8 to 3.2. We found that a good description of various small clusters, as those of Refs. 29 and 30, required different angular functions for the coordinations two and three. Simulations for the liquid phase^{23,28} suggest that a weakening of the angular correlation for small angles is required for higher coordinations as well. For LCBOP we have formulated a dynamic coordination dependence which smoothly interpolates the angular correlation for coordinations $N_{ijk} \leq 8$.

TABLE I. Parameters of the LCBOPII. The units of energy and length are eV and Å, respectively.

Switch	q	q_{min}	q_{max}	p	Switch	q	q_{min}	q_{max}	p	Switch	q	q_{min}	q_{max}	p
S_{sr}^{down}	r_{ij}	1.7	2.2	3.0	S_{mr}^{sup}	r_{ij}	1.7	2.2	-2.0	S_N^{down}	r_{ij}	1.7	2.2	-3.0
S_{lr}^{down}	r_{ij}	5.5	6.0	0	S_M^{sup}	N_{ki}	2.0	3.0	0	S_{sat}^{down}	N_{ki}	3.0	4.0	0
S_{db}^{down}	x_{ij}^{db}	0.0	1.0	0	$S_{\gamma,0}^{up}$	γ_{ij}	0.34	0.93	0	$S_{\gamma,2}^{up}$	γ_{ij}	0.30	0.93	0
Short-range potential V^{sr}														
V_R	$A^{sr}=53026.92614 \quad \alpha=6.74750993$													
V_A	$B_1^{sr}=27618.35706 \quad \beta_1=6.34503890 \quad B_2^{sr}=34.07142502 \quad \beta_2=1.19712839$													
G	$g_{min}=0.0020588719 \quad g_{gr}=0.0831047003 \quad g_{max}=16.0$													
	$g_{1,0}=0.7233666272 \quad g_{1,1}=1.7334665088 \quad g_{1,2}=1.8701997632$													
	$g_{2,0}=0.73994527795 \quad g_{2,1}=-1.999211817 \quad g_{2,2}=-17.43251545$													
	$g_{2,3}=-33.96127110 \quad g_{2,4}=-44.65392079$													
	$g_{3,0}=-15.19 \quad g_{3,1}=-25.6168552398 \quad g_{3,2}=-21.51728397$													
	$g_{3,3}=0.9899080993 \quad g_{3,4}=13.66416160$													
	$A_{y_0}=-0.4 \quad B_{y_0}=0.01875$													
	$A_g=5.6304664723 \quad B_g=0.1516943990 \quad C_g=0.009832975891$													
	$D_g=-0.189175977654 \quad E_g=0.050977653631$													
H	$d=0.14 \quad C_1=3.335 \quad C_4=220.0$ For C_6, L, κ, R_0 and R_1 see text.													
F_{ij}^{conj}	$F_{ij,0}^{conj} \quad F_{ij,1}^{conj}$													
	0.0000	0.0207	-0.0046	-0.1278	0.0000	0.0584	0.0416	-0.1278						
	0.0207	0.0000	-0.0365	-0.1043	0.0584	0.1379	0.0062	-0.1243						
	-0.0046	-0.0365	0.0000	-0.0273	0.0416	0.0062	0.0936	-0.0393						
	-0.1278	-0.1043	-0.0273	0.0000	-0.1278	-0.1243	-0.0393	0.0000						
A_{ij}	$\alpha_0=0.95$													
T_{ij}	$A_t=-13.152909887$													
	$B_{t1}=-0.0486839616 \quad B_{t2}=3.8 \quad B_{t3}=0.62 \quad B_{t4}=0.005$													
Long-range potential V^{lr}														
$\tau_0=3.715735 \quad \epsilon_1=0.002827918 \quad \lambda_1=1.338162 \quad \lambda_2=2.260479$ For ϵ_1, v_1 , and v_2 see text.														
Middle-range potential V^{mr}														
$r_1^{mr}=4.0 \quad r_2^{mr}=2.9 \quad A_0^{mr}=-0.2345 \quad A_1^{mr}=-0.67 \quad A_2^{mr}=-4.94$														

Using the short notations $y=\cos \theta_{ijk}$ and $z=N_{ijk}$, the angular function $G(y,z)$ reads

$$G(y,z) = \Theta(y_0(z)-y)G_1(y) + \Theta(y-y_0(z))G_2(y,z), \quad (12)$$

where $G_1(y)$ is the angular function fitting the properties of the various bulk crystal lattices from chain to fcc as in LCBOP1,²² and $G_2(y,z)$ gives a weaker angular correlation, as compared to $G_1(y,z)$, for low coordinations and small angles. The function G is presented in Fig. 3. The coordination dependent boundary value $y_0(z)$ where G_2 is smoothly matched to G_1 is given by

$$y_0(z) = A_{y_0} + B_{y_0}(z+z^2). \quad (13)$$

For high coordination $y_0(z)$ becomes larger than one and $G(y,z)=G_1(y)$ for all angles. The functions $G_1(y)$ and $G_2(y,z)$ are given by

$$G_1(y) = \begin{cases} g_{min} + (y+1)^2 \sum_{n=0}^2 g_{1,n} y^n, & -1 \leq y < -\frac{1}{2} \\ g_{gr} + \left(y + \frac{1}{2}\right) \sum_{n=0}^4 g_{2,n} y^n, & -\frac{1}{2} \leq y < -\frac{1}{3} \\ g_{max} + (y-1)^2 \sum_{n=0}^4 g_{3,n} y^n, & -\frac{1}{3} \leq y \leq 1 \end{cases} \quad (14)$$

and

$$G_2(y,z) = g_{z,max} + (1-y)^2 \sum_{n=0}^2 g_{z,n} y^n \quad (15)$$

respectively, where

$$g_{z,max} = g_{max} - (A_g + B_g z + C_g z^4)(1-y_0)^3 \quad (16)$$

and

$$g_{z,2} = \frac{D_g z^4}{1 + E_g z^4}. \quad (17)$$

The coefficients $g_{z,0}$ and $g_{z,1}$ are fixed by the requirement of continuity of $G(y,z)$ up to the first derivative at $y=y_0(z)$, implying

$$g_{z,1} = \frac{G'_1(y_0)}{(y_0 - 1)^2} - 2 \frac{G_1(y_0)}{(y_0 - 1)^3} - 2g_{z,2}y_0 \quad (18)$$

and

$$g_{z,0} = \frac{G_1(y_0) - g_{z,max}}{(y_0 - 1)^2} - g_{z,1}y_0 - g_{z,2}y_0^2, \quad (19)$$

where $G'_1(y_0) = dG_1/dy|_{y_0}$.

The function $H(\delta r_{ijk})$ shown in Fig. 3 is almost the same as for LCBOP1 and reads

$$H(x) = \begin{cases} H_1(x) = L \left[1 + \kappa(x+d) \left(\frac{1}{1 + [\kappa(x+d)]^4} \right)^{1/4} \right], & x < -d \\ H_2(x) = 1 + C_1x + \frac{1}{2}C_1^2x^2 + C_4x^4 + C_6x^6, & -d \leq x \leq d \\ H_3(x) = R_0 + R_1(x-d), & x > d \end{cases} \quad (20)$$

with three independent parameters d , C_1 , and C_4 and where L , κ , C_6 , R_0 , and R_1 follow from continuity of H up to its second derivative at $x=\pm d$. By construction $d^2H_1/dx^2|_{x=-d} = d^2H_3/dx^2|_{x=d} = 0$ so that C_6 follows directly from $d^2H_2/dx^2|_{x=-d} = d^2H_2/dx^2|_{x=d} = 0$. Next L and R_0 follow from continuity of H in $x=-d$ and $x=d$, respectively, leaving R_1 and κ to be found from continuity of the first derivative of H at $x=\pm d$.

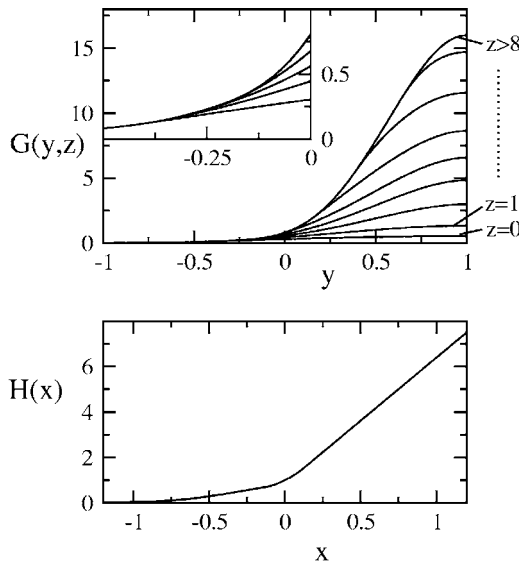


FIG. 3. Top panel: function $G(y,z)$ [Eq. (12)] for integer values of z . The inset shows that G_2 is smoothly matched to G_1 at a coordination dependent boundary value $y_0(z)$; the vertical axis of the inset is labeled on the right-hand side. Bottom panel: function $H(x)$ [Eq. (20)].

2. Conjugation term F_{ij}^{conj}

We call atom j a full neighbor of atom i if $S_{N,ij}^{down} = 1$. If $0 < S_{N,ij}^{down} < 1$ then atom j is called a fractional neighbor. For LCBOP1, as for Brenner's potentials, F_{ij}^{conj} is a function of the reduced coordination numbers N_{ij} and N_{ji} , and of the conjugation number N_{ij}^{conj} . The number N_{ij} is defined by

$$N_{ij} = N_i - S_{N,ij}^{down}. \quad (21)$$

The values of F_{ij}^{conj} for integer N_{ij} and N_{ji} were fitted to known bond energies for equilibrium configurations with appropriate coordination environments.^{15,22} A cubic spline was used to extend F_{ij}^{conj} to noninteger coordinations. In this interpolation approach, a situation where atom i has two full neighbors other than j gives the same argument $N_{ij}=2$ as a situation where atom i has one full neighbor other than j and two fractional neighbors $k_1 \neq j$ and $k_2 \neq j$ with $S_{N,ik_1}^{down} + S_{N,ik_2}^{down} = 1$ which can lead to unreasonable values for F_{ij}^{conj} . Therefore, for LCBOP1, which we wish to be applicable also to the liquid phase where multiple fractional neighbors often occur, we propose an interpolation scheme which makes use only of the values of F_{ij}^{conj} for integer N_{ij} and N_{ji} . In this new approach, the above situation is interpolated as a weighted sum of one configuration with $N_{ij}=1$ (both fractional neighbors excluded), two configurations with $N_{ij}=2$ (one of the fractional neighbors included as a full neighbor and the other excluded and vice versa) and one configuration with $N_{ij}=3$ (both fractional neighbors included as full neighbors). Mathematically, this can be written as

$$F_{ij}^{conj} = \sum_{\{\sigma_k=0,1\}} \sum_{\{\sigma_f=0,1\}} W_{ij,\{\sigma_k\}} W_{ji,\{\sigma_f\}} \times F_{ij}^{conj}(\tilde{N}_{ij,\{\sigma_k\}}, \tilde{N}_{ji,\{\sigma_f\}}, N_{ij,\{\sigma_k\}\{\sigma_f\}}^{conj}) \quad (22)$$

where

$$W_{ij,\{\sigma_k\}} = \prod_{k \neq i,j} (\sigma_k S_{N,ik}^{\text{down}} + (1 - \sigma_k)(1 - S_{N,ik}^{\text{down}})) \quad (23)$$

is a weight factor. The summation $\sum_{\{\sigma_k=0,1\}}$ runs over all possible sets of numbers $\{\sigma_k\}$, one number for each neighbor $k \neq j$ of i , with each σ_k assuming the value 0 or 1. Note, however, that $W_{ij,\{\sigma_k\}}=0$ for all sets $\{\sigma_k\}$ containing a $\sigma_k=0$ for a full neighbor $k \neq j$ of i . Therefore the summation can be restricted to the fractional neighbors, putting $\sigma_k=1$ for all full neighbors. The expression (22) requires only the values of F^{conj} for the integer arguments $\tilde{N}_{ij,\{\sigma_k\}}$ (ranging between 0 and 3), defined as

$$\tilde{N}_{ij,\{\sigma_k\}} = \min(3, N_{ij,\{\sigma_k\}}) \quad (24)$$

with

$$N_{ij,\{\sigma_k\}} = \sum_{k \neq i,j} \sigma_k. \quad (25)$$

The definition of the conjugation number $N_{ij,\{\sigma_k\}\{\sigma_l\}}^{\text{conj}}$ is equivalent to that for LCBOP, but is presented here in a more transparent form. By construction it is a number between 0 and 1 and reads

$$N_{ij,\{\sigma_k\}\{\sigma_l\}}^{\text{conj}} = \frac{N_{ij}^{\text{el}} + N_{ji}^{\text{el}} - N_{ij,\text{min}}^{\text{el}} - N_{ji,\text{min}}^{\text{el}}}{N_{ij,\text{max}}^{\text{el}} + N_{ji,\text{max}}^{\text{el}} - N_{ij,\text{min}}^{\text{el}} - N_{ji,\text{min}}^{\text{el}} + \epsilon}, \quad (26)$$

where N_{ij}^{el} is the fractional number of electrons supplied by atom i to the bond ij given by

$$N_{ij}^{\text{el}} = \frac{4 - \tilde{M}_{ij,\{\sigma_k\}}}{\tilde{N}_{ij,\{\sigma_k\}} + 1 - \tilde{M}_{ij,\{\sigma_k\}}} \quad (27)$$

with $\tilde{M}_{ij,\{\sigma_k\}}$ the fractional number of saturated (i.e., with coordination at least four) neighbors $k \neq j$ of atom i . It is defined by

$$\tilde{M}_{ij,\{\sigma_k\}} = \min(3, M_{ij,\{\sigma_k\}}) \quad (28)$$

where $M_{ij,\{\sigma_k\}}$ is given by

$$M_{ij,\{\sigma_k\}} = \sum_{k \neq i,j} \sigma_k S_M^{\text{up}}(N_{ki}) \quad (29)$$

with $N_{ki} = N_k - S_{N,ki}^{\text{down}}$ according to Eq. (21). According to these definitions the minimal and maximal values of N_{ij}^{el} , to be inserted into Eq. (26), are given by

$$N_{ij,\text{min}}^{\text{el}} = \frac{4}{\tilde{N}_{ij,\{\sigma_k\}} + 1} \quad \text{and} \quad N_{ij,\text{max}}^{\text{el}} = 4 - \tilde{N}_{ij,\{\sigma_k\}}, \quad (30)$$

respectively. We assume a linear dependence of $F_{ij,\{\sigma_k\}\{\sigma_l\}}^{\text{conj}}$ on $N_{ij,\{\sigma_k\}\{\sigma_l\}}^{\text{conj}}$, i.e.,

$$F_{ij,\{\sigma_k\}\{\sigma_l\}}^{\text{conj}} = (1 - N_{ij,\{\sigma_k\}\{\sigma_l\}}^{\text{conj}}) F_{ij,0}^{\text{conj}} + N_{ij,\{\sigma_k\}\{\sigma_l\}}^{\text{conj}} F_{ij,1}^{\text{conj}} \quad (31)$$

with $F_{ij,0}^{\text{conj}} = F^{\text{conj}}(\tilde{N}_{ij,\{\sigma_k\}}, \tilde{N}_{ji,\{\sigma_l\}}, 0)$ and $F_{ij,1}^{\text{conj}} = F^{\text{conj}}(\tilde{N}_{ij,\{\sigma_k\}}, \tilde{N}_{ji,\{\sigma_l\}}, 1)$ given in Table I. In Eq. (26), ϵ is a very small positive number that prevents the numerical

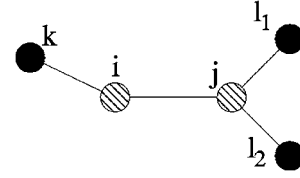


FIG. 4. Example used to describe the term A_{ij} that accounts for occupancy of antibonding states (see text).

singularities occurring for coordination combinations $(\tilde{N}_{ij,\{\sigma_k\}}, \tilde{N}_{ji,\{\sigma_l\}}) = (0,0), (0,3), (3,0)$, and $(3,3)$, where $N_{ij,\{\sigma_k\}\{\sigma_l\}}^{\text{conj}} = 0/\epsilon = 0$. Actually, for these combinations $F_{ij,0}^{\text{conj}} = F_{ij,1}^{\text{conj}}$ so that the value of $N_{ij,\{\sigma_k\}\{\sigma_l\}}^{\text{conj}}$ becomes irrelevant.

3. Antibonding term A_{ij}

The term A_{ij} accounts for occupancy of antibonding states. When the supply of electrons from atom i to the bond ij , N_{ij}^{el} , is not equal to that from atom j , N_{ji}^{el} , bonding is relatively less effective. To illustrate this point, we refer to the situation shown in Fig. 4. For the ij -bond with $N_{ij,\{\sigma_k\}} = 1$ and $N_{ji,\{\sigma_l\}} = 2$ with saturated neighbors $k \neq j$ of i and $l \neq i$ of j , yielding $N_{ij,\{\sigma_k\}\{\sigma_l\}}^{\text{conj}} = 1$, we have $N_{ij}^{\text{el}} = 3$ and $N_{ji}^{\text{el}} = 2$. Instead of a bond energy somewhere between that of a double bond (6.2 eV, Ref. 16) and that of a triple bond (8.4 eV, Ref. 16), the bond energy for this bond is only about 5.8 eV, according to LCBOP, LCBOP2, and REBO, due to the unfavorable situation that not all electrons can make pairs, giving rise to an antibonding state being occupied by the lone electron. Conversely, if the neighbors k and l are unsaturated, yielding $N_{ij,\{\sigma_k\}\{\sigma_l\}}^{\text{conj}} = 0$, the bond energy is equal to 5.2 eV. With the linear dependence in Eq. (31), the bond energy of this bond for $0 < N_{ij,\{\sigma_k\}\{\sigma_l\}}^{\text{conj}} < 1$ is always between 5.2 and 5.8 eV for LCBOP and REBO. However, when the two neighbors $l \neq i$ of atom j are saturated and the neighbor $k \neq j$ of atom i is unsaturated, we have $N_{ij}^{\text{el}} = 2$ and $N_{ji}^{\text{el}} = 2$, i.e., a proper double bond which should have a bond energy of about 6.2 eV. For this case, $N_{ij,\{\sigma_k\}\{\sigma_l\}}^{\text{conj}} = 2/5$. In order to describe all these situations correctly we introduced the antibonding term A_{ij} , which, using the same interpolation approach as for the conjugation term, is given by

$$A_{ij} = \sum_{\{\sigma_k=0,1\}}' \sum_{\{\sigma_l=0,1\}}' W_{ij,\{\sigma_k\}} W_{ji,\{\sigma_l\}} a_{ij}(\Delta_{el}), \quad (32)$$

where the summations are restricted to those configurations with $(N_{ij,\{\sigma_k\}}, N_{ji,\{\sigma_l\}})$ equal to (1,1), (2,2), (1,2), or (2,1) and where

$$a_{ij}(\Delta_{el}) = \frac{\alpha_0 \Delta_{el}^2}{1 + 10|\Delta_{el}|} \quad (33)$$

with

$$\Delta_{el} = N_{ij,\{\sigma_k\}}^{\text{el}} - N_{ji,\{\sigma_l\}}^{\text{el}}. \quad (34)$$

The function a_{ij} tends to a linear dependence on $|\Delta_{el}|$ while being continuous up to the first derivative at $\Delta_{el}=0$. For $(N_{ij,\{\sigma_k\}}, N_{ji,\{\sigma_l\}})$ not equal to (1,1), (2,2), (1,2), or (2,1) the

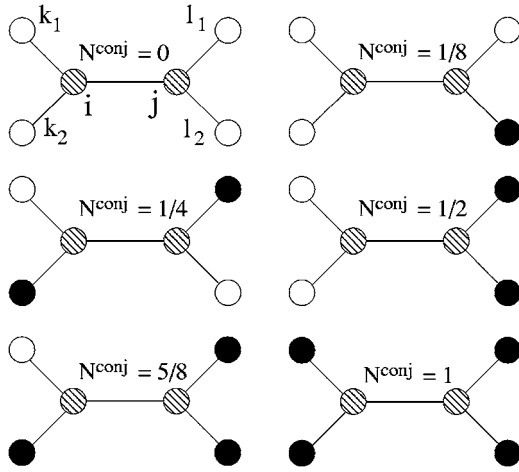


FIG. 5. Schematic molecules with a central bond between two sp_2 sites (i and j , dashed circles), for all the possible values of N^{conj} [Eq. (26)] with integer coordinated neighbors. White circles represent threefold- sp_2 sites, while black circles are for fourfold- sp_3 sites.

linear interpolation Eq. (31) is reasonable and the correction A_{ij} is not required.

4. Torsion term T_{ij}

Also for the torsion term T_{ij} , the same interpolation approach is used as for the conjugation term:

$$T_{ij} = \sum_{\{\sigma_k=0,1\}}'' \sum_{\{\sigma_l=0,1\}}'' W_{ij,\{\sigma_k\}} W_{ji,\{\sigma_l\}} t_{ij}(\gamma_{ij,\{\sigma_k\}\{\sigma_l\}}, N_{ij,\{\sigma_k\}\{\sigma_l\}}^{conj}), \quad (35)$$

where now the summations are restricted only to those configurations with $(N_{ij,\{\sigma_k\}}, N_{ji,\{\sigma_l\}}) = (2, 2)$. The torsional term t_{ij} for each of these configurations depends on $\gamma_{ij,\{\sigma_k\}\{\sigma_l\}} = \cos(\omega_{ij,\{\sigma_k\}\{\sigma_l\}})$ with $\omega_{ij,\{\sigma_k\}\{\sigma_l\}}$ the torsion angle and on the conjugation number $N_{ij,\{\sigma_k\}\{\sigma_l\}}^{conj}$ for this configuration. The DF calculations of the torsional barrier for the six cases of Fig. 5, shown in Fig. 6, display a rather complex dependence of the torsional barrier on each of the possible conjugation numbers. Fitting this behavior led us to the following form for t_{ij} :

$$t_{ij}(\tilde{\gamma}, \tilde{z}) = \begin{cases} \tau_1(\tilde{z})(\tilde{\gamma}^2(1-\tilde{\gamma}^2))^2, & \tilde{z} \leq \frac{1}{8} \\ \tau_2(\tilde{z})(1-\tilde{\gamma}^2)(2-\tilde{\gamma}^2)^2, & \tilde{z} > \frac{1}{8}, \end{cases} \quad (36)$$

where we used the short notations $\tilde{\gamma} = \cos(\omega_{ij,\{\sigma_k\}\{\sigma_l\}})$ and $\tilde{z} = N_{ij,\{\sigma_k\}\{\sigma_l\}}^{conj}$ and where

$$\tau_1(\tilde{z}) = A_t(\tilde{z} - 1/8)^2, \quad (37)$$

$$\tau_2(\tilde{z}) = \frac{B_{t1}(\tilde{z} - 1/8)^2(\tilde{z} + B_{t2}\Delta_{el}^2[\Delta_{el}^2 - (2/3)^2])^2(1 - B_{t3}\tilde{z})}{B_{t4} + (\tilde{z} - 1/8)^2}. \quad (38)$$

For LCBOP⁺ (see Appendix A) the torsion angle was defined as the angle between the vector product of \mathbf{r}_{ij} with \mathbf{r}_{ik} and the vector product of \mathbf{r}_{ij} with \mathbf{r}_{jl} , as for the REBO po-

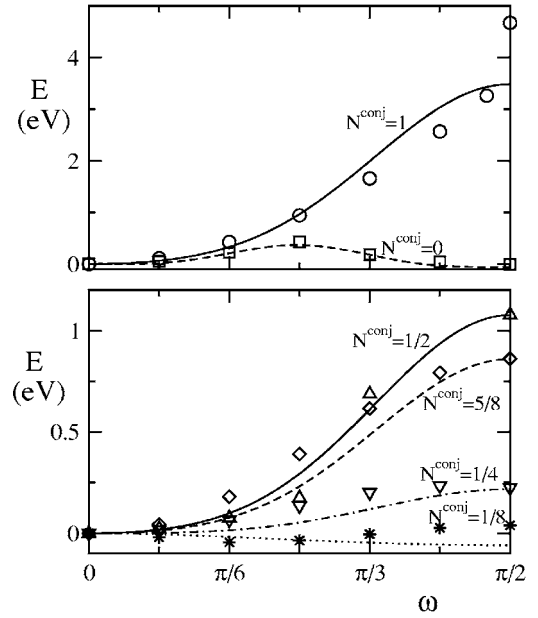


FIG. 6. Torsional barriers according to LCBOP2 and our DF calculations for the six values of N^{conj} corresponding to the molecules schematically represented in Fig. 5. Symbols represent the DF results, and curves represent the fits obtained by the LCBOP2. Top panel: torsional barriers for the extreme values of N^{conj} , corresponding to the conjugated ($N^{conj}=0$, squares and dashed curve) and double bonds ($N^{conj}=1$, circles and solid curve). Bottom panel: intermediate values of N^{conj} : $1/8$ (stars and dotted curve), $1/4$ (down triangles and dashed-dotted curve), $1/2$ (up triangles and solid curve), and $5/8$ (diamonds and dashed curve). Note the complex behavior of the curves for the values $1/2$ and $5/8$, where the barrier at $\pi/2$ is higher for $N^{conj}=1/2$ than for $N^{conj}=5/8$.

tential. The total torsion term T_{ij} was the sum of contributions from the torsion angles from all pairs of these vector products. However, apart from the problematic singularity occurring when \mathbf{r}_{ik} or \mathbf{r}_{jl} is parallel to \mathbf{r}_{ij} this definition of the torsion term gives a nonzero torsion for many situations, like the one shown in Fig. 7, where there is actually no torsion at all. For example, it gives a nonzero torsion for the dimer bond on the reconstructed (001) surface, leading to a too large dimer bond distance (1.555 Å for the LCBOP⁺ and 1.546 Å for the REBO potential against the experimental value 1.37 Å). Therefore for LCBOP2 we have formulated a different expression for the torsion angle which does not give “spurious torsion” and interpolates well for any configuration. For each configuration where two bonded atoms i and j both have two other neighbors (k_1, k_2) and (l_1, l_2), respectively, characterized by the two sets of numbers $\{\sigma_k\}$ and $\{\sigma_l\}$, we define a single torsion angle through

$$\tilde{\gamma} = \cos(\omega_{ij,\{\sigma_k\}\{\sigma_l\}}) = \frac{\mathbf{t}_{ijk} \cdot \mathbf{t}_{jil}}{|\mathbf{t}_{ijk}| |\mathbf{t}_{jil}|} \quad (39)$$

where the vector \mathbf{t}_{ijk} is given by

$$\mathbf{t}_{ijk} = \hat{\mathbf{r}}_{ij} \times \hat{\mathbf{w}}_{ijk}^- + (\hat{\mathbf{r}}_{ij} \cdot \hat{\mathbf{w}}_{ijk}^-)(\hat{\mathbf{r}}_{ij} \times \hat{\mathbf{w}}_{ijk}^+) \quad (40)$$

with

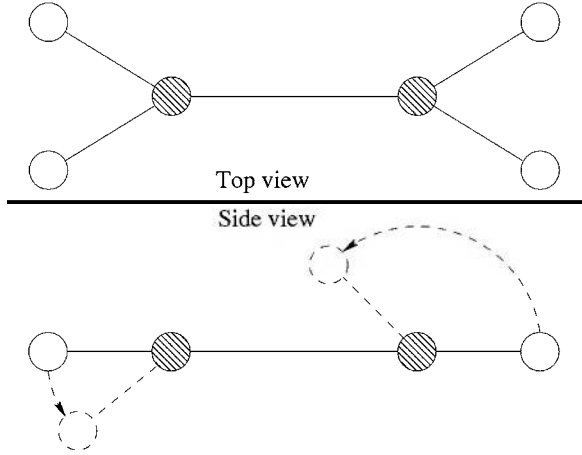


FIG. 7. Scheme to show a case with no torsion, according to our definition. Starting from the molecule in its planar configuration, out of plane bending described by dashed arrows leaves $\tilde{\gamma}=0$, thus giving the torsional term $T_{ij}=0$. Only the twisting around the central bond gives a $\tilde{\gamma} \neq 0$. In contrast, previous definitions of the torsion angle, such as in Refs. 16, 20, and 42, give a spurious nonzero torsional contribution for the bending shown in this figure.

$$\hat{\mathbf{w}}_{ijk}^- = \frac{\hat{\mathbf{r}}_{ik_1} - \hat{\mathbf{r}}_{ik_2}}{|\hat{\mathbf{r}}_{ik_1} - \hat{\mathbf{r}}_{ik_2}|}, \quad \hat{\mathbf{w}}_{ijk}^+ = \frac{\hat{\mathbf{r}}_{ik_1} + \hat{\mathbf{r}}_{ik_2}}{|\hat{\mathbf{r}}_{ik_1} + \hat{\mathbf{r}}_{ik_2}|} \quad (41)$$

and $\hat{\mathbf{r}}_{ij} = \mathbf{r}_{ij}/|\mathbf{r}_{ij}|$. We note that the definition Eq. (40) becomes equivalent to the one of REBO for the standard case of rotation around the axis $\hat{\mathbf{r}}_{ij}$.

C. Long-range potential V^{lr}

The functional form of the long-range pair potential V_{ij}^{lr} is the same as for LCBOP1:

$$V^{lr}(r) = [\theta(r_0 - r)V_1^{lr}(r) + \theta(r - r_0)V_2^{lr}(r)]S_{lr}^{down}(r) \quad (42)$$

where V_i^{lr} ($i=1,2$) are ordinary Morse functions plus a shift:

$$V_i^{lr}(r) = \epsilon_i(e^{-2\lambda_i(r-r_0)} - 2e^{-\lambda_i(r-r_0)}) + v_i \quad (43)$$

and $S_{lr}^{down}(r)$ smoothly cuts off the long-range interactions at 6 Å. The two Morse functions are connected continuously up to the second derivative in $r=r_0$, implying $\epsilon_1 = \epsilon_2\lambda_2^2/\lambda_1^2$ and $v_1 = \epsilon_1 - \epsilon_2$ with $v_2=0$. The values of the parameters have slightly changed as compared to those for LCBOP1, leading to an optimal fit of the compressibility in the direction perpendicular to the layers, namely $4.324 \times 10^{-3} \text{ Å}^3/\text{meV}$ to be compared to the experimental value $4.326 \times 10^{-3} \text{ Å}^3/\text{meV}$.^{31,32} This long-range part binds the graphitic layers at the experimental equilibrium distance of 3.35 Å, the binding energy being 25 meV/atom.²²

D. Middle-range potential

The middle-range attractive interactions in Eq. (1), representing an important novelty of LCBOP2, are environment dependent. They depend on bond angles and on the presence of “dangling bonds” as quantified by the dangling bond number N^{db} defined in the following. It reads:

$$V_{ij}^{mr} = \begin{cases} S_{db}^{down}(x_{ij}^{db})S_{\gamma,0}^{sup}(\gamma_{ij})V_{0,ij}^{mr} + S_{db}^{up}(x_{ij}^{db})\tilde{S}_{\gamma,1}^{sup}(\gamma_{ij})V_{1,ij}^{mr}, & 0 \leq N_{ij}^{db} \leq 1 \\ S_{db}^{down}(x_{ij}^{db})\tilde{S}_{\gamma,1}^{sup}(\gamma_{ij})V_{1,ij}^{mr} + S_{db}^{up}(x_{ij}^{db})S_{\gamma,2}^{sup}(\gamma_{ij})V_{2,ij}^{mr}, & 1 < N_{ij}^{db} \leq 2 \\ S_{db}^{down}(x_{ij}^{db})S_{\gamma,2}^{sup}(\gamma_{ij})V_{2,ij}^{mr}, & 2 < N_{ij}^{db} \leq 3, \end{cases} \quad (44)$$

where

$$x_{ij}^{db} = N_{ij}^{db} - I_{ij}^{db} \quad (45)$$

with $I_{ij}^{db} = \text{Int}(N_{ij}^{db})$ (i.e., the largest integer smaller than N_{ij}^{db}). The dangling bond number N_{ij}^{db} is defined as

$$N_{ij}^{db} = 4 - \sum_{k \neq i,j} S_{N_{ik}}^{down} N_{ki}^{el}, \quad (46)$$

where N_{ki}^{el} is the number of electrons from atom k available for the bond ki , defined by

$$N_{ki}^{el} = \frac{4 - S_{sat}^{down}(N_{ki})M_{ki}}{N_{ki} + 1 - S_{sat}^{down}(N_{ki})M_{ki}} \quad (47)$$

with

$$M_{ki} = \sum_{m \neq k,i} S_N^{down}(r_{km})S_M^{up}(N_{mk}) \quad (48)$$

and $S_{sat}^{down}(N_{ki})$ goes to zero for $N_{ki} \geq 3$, i.e., when atom k is saturated.

In Eq. (44) the attractive potentials $V_{n,ij}^{mr} = V_n^{mr}(r_{ij})$ are simple polynomials cut off smoothly:

$$V_n^{mr}(r_{ij}) = A_n^{mr}\Theta(r_1^{mr} - r_{ij})(r_1^{mr} - r_{ij})^3, \quad (49)$$

$$V_2^{mr}(r_{ij}) = A_2^{mr}\Theta(r_2^{mr} - r_{ij})(r_2^{mr} - r_{ij})^2, \quad (50)$$

for situations with $n=0,1$ dangling bond, and 2 dangling bonds, respectively. For $N_{ij}^{db} \geq 3$ we set $V_{ij}^{mr}=0$. In the presence of dangling bond(s) (with $N_{ij}^{db} < 3$) the middle-range attraction is stronger than without dangling bond(s). The parameter γ_{ij} is related to the bond angles by

$$\gamma_{ij} = \frac{1}{1 + (B/N_{ij}) \sum_{k \neq i,j} (1 + \cos \theta_{ijk})^4}. \quad (51)$$

For small angles, γ_{ij} becomes small. If γ_{ij} is smaller than the lower bounds of the switch functions $S_{\gamma,n}^{up}$, then $V_{ij}^{mr}=0$ according to Eq. (44). According to the definition of N_{ij}^{ab} , $N_{ij}^{ab}=0$ for each of the equilibrium bulk phases, i.e., chain, graphite, diamond, etc. The lower bound of $S_{\gamma,0}^{up}$ is chosen such that the middle-range interaction vanishes for each of these bulk phases. So the middle-range interaction does not affect the equilibrium properties of these phases to which the short-range potential, combined with the given V^{lr} , is fitted, but it only affects the energetics for bond breaking and formation. The lower bound for the switch functions $S_{\gamma,n}^{up}$ depends also on the dangling bond number, favoring the attraction when dangling bond(s) are involved. In order to make the attraction for a single bond more directional than that for a double bond, we took

$$\tilde{S}_{\gamma,1}^{up} = (S_{\gamma,2}^{up})^2. \quad (52)$$

The middle-range coordination number Z_i^{mr} is defined as

$$Z_i^{mr} = \left(\frac{\left(\sum_j \tilde{v}_{ij} \right)^2}{\sum_j \tilde{v}_{ij}^2} \right)^{\delta_{mr}} \quad (53)$$

where we used the short notation $\tilde{v}_{ij} = S_{mr,ij}^{up} V_{ij}^{mr}$ and where δ_{mr} is a correlation exponent. The larger δ_{mr} , the larger Z_i^{mr} , the stronger is the middle-range correlation. Without this correlation (i.e., $\delta_{mr}=0$) the middle-range contribution tends to become too large and gives unrealistic configurations with accumulation of atoms in the middle range. On the basis of simulations for the liquid phase at various densities, we took $\delta_{mr}=1/2$. With this exponent the middle-range correlation is equivalent with the correlation in the embedded atom potentials and the total middle-range energy of atom i becomes

$$E_i^{mr} = \frac{1}{2} \sum_j \tilde{v}_{ij} = \frac{1}{2} \sqrt{\frac{\sum_j \tilde{v}_{ij}^2}{\left(\sum_j \tilde{v}_{ij} \right)^2}} \sum_j \tilde{v}_{ij} = -\frac{1}{2} \left(\sum_j \tilde{v}_{ij}^2 \right)^{1/2}. \quad (54)$$

The minus sign appears due to the fact that $\tilde{v}_{ij} \leq 0$ for all pairs ij . With this MR contribution, a reasonable agreement of the dissociation energy curves calculated by LCBOP2 and by DF is obtained, as shown in Fig. 8 for single, double, and triple bonds. All parameters of LCBOP2 are given in Table I.

III. PROPERTIES

The potential LCBOP2 accounts by construction for the structural and elastic properties of most crystalline structures of carbon and for these quantities gives values very close to LCBOP1.²² Conversely, it gives a more accurate description of more complex structures, such as the reconstructed surfaces of diamond, and of the energetics of phase transformations and structural defects.

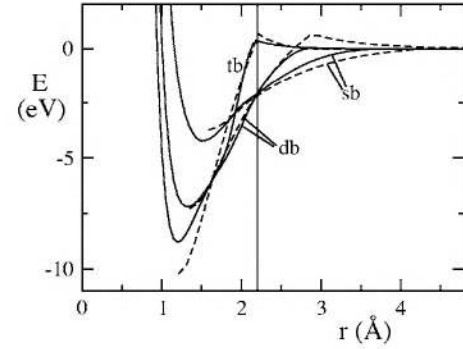


FIG. 8. Bonding energy for $(\text{CH}_3)\text{C}\equiv\text{C}(\text{CH}_3)$ (triple bond, tb), $(\text{CH}_3)_2\text{C}=\text{C}(\text{CH}_3)_2$ (double bond, db), and $(\text{CH}_3)_3\text{C}-\text{C}(\text{CH}_3)_3$ (single bond, sb), calculated by DF (dashed curves) and LCBOP2 (solid curves) as described in the text. To determine the parameters A_1^{mr} and A_2^{mr} of Eq. (50), we impose the energy of the central single and double bonds, stretched to 2.2 Å (vertical line), to be equal to the corresponding DF value.

A. Bulk equilibrium structures and elastic constants

In Table II we give the values of the equilibrium interatomic distance d_{CC} , binding energy E_b , and stretching force constant F_c for different crystalline structures, compared to the reference values of Refs. 15, 16, 33, and 34. Table II can be directly compared to Table I of Ref. 22 containing also the values for LCBOP1 and REBO. The values of LCBOP1+ are the same as for LCBOP1. In Table III we give the elastic force constants for diamond and graphite compared to the results of Refs. 35 and 36, respectively.

B. Diamond (111) and (001) reconstructed surfaces

The energy and structure of crystalline surfaces results from a delicate balance of forces due to undercoordinated atoms at the surface and represent a severe test for interatomic potentials. In Table IV we give the surface energy and the interatomic distances of the relaxed (2×1) -Pandey-reconstructed (111) and of the (2×1) reconstructed (001)

TABLE II. Bond distances d_{CC} , binding energies E_b , and stretching force constants F_c calculated by LCBOP2 for the coordination Z of a C_2 dimer bond (di), a linear chain (ch), the triple bond (tb) and the crystalline structures graphite (gr), diamond (d), simple cubic (sc), and face centered cubic (fcc). The binding energy for graphite includes the interlayer binding energy described by V_{lr} . In parentheses we give the reference values of Refs. 15, 16, 33, and 34.

Z	d_{CC} (Å)	E_b (eV/atom)	F_c (eV/Å ²)
1 (di)	1.315 (1.315)	3.081 (3.163)	
2 (ch)	1.325 (1.330)	6.089 (6.175)	62.29 (59.67)
2 (tb)	1.200 (1.200)	8.524 (8.424)	98.85 (99.86)
3 (gr)	1.420 (1.420)	7.374 (7.374)	43.95 (43.57)
4 (d)	1.544 (1.544)	7.349 (7.349)	29.27 (29.52)
6 (sc)	1.770 (1.765)	4.760 (4.689)	
12 (fcc)	2.170 (2.170)	2.759 (2.759)	

TABLE III. Elastic force constants (in eV/Å³) for graphite (gr) and diamond (d). In parentheses we give the reference values of Ref. 36 for graphite and Ref. 35 for diamond.

c_{11} (gr)	6.551 (6.616)
c_{66} (gr)	2.763 (2.746)
c_{11} (d)	6.718 (6.718)
c_{44} (d)	3.604 (3.604)

surfaces, with the same notation of Fig. 6 and Table IV of Ref. 22. It is important to notice that the (2×1) reconstruction of the (001) surface does not imply any torsion of the bonds whereas a torsional contribution is present for the $(111)(2 \times 1)$. With the definition of torsion of LCBOPH both situations are correctly described, whereas REBO and LCBOPH⁺ give a spurious torsion for the $(001)(2 \times 1)$ surface, leading to the too large value of the d_{12} distance (see Table IV).

C. Graphite to diamond transformation

The transformation from graphite to diamond occurs via a reaction path that can be parametrized by one reaction coordinate, the carbon-carbon distance $r_{CC,\perp}$ between two atoms in adjacent (111) bilayers evolving towards graphitic planes. The *ab initio* results of Fahy *et al.*,³⁷ for the energy barrier E , intraplanar carbon-carbon distance $r_{CC,\parallel}$, and buckling angle θ are compared in Fig. 9 with the results of LCBOPH and also LCBOPH⁺. Notice that only the barrier height has been used in the fitting procedure as it has been done also for LCBOPH. The structural details of the transformation along

TABLE IV. Surface energy [in eV/(unit cell of the unreconstructed surface)] and interatomic distances (in Å) of the relaxed (2×1) -Pandey-reconstructed (111) and of (2×1) reconstructed (001) surfaces, with the same notation of Fig. 6 and Table IV of Ref. 22. Notice that the REBO data in Table IV of Ref. 22 are indicated here as REBO* and refer to the REBO potential without torsional interactions, i.e., with $b_{ij}^{DH}=0$.

	Reference	LCBOPH	REBO*	REBO	LCBOPH ⁺
(111)(2 × 1)					
E_{surf}	1.87	1.2807	1.01	1.91	1.59
d_{12}	1.43	1.460	1.437	1.445	1.455
d_{13}	1.54	1.539	1.559	1.527	1.535
d_{24}	1.54	1.540	1.565	1.534	1.545
d_{35}	1.61 1.62	1.643	1.621	1.644	1.626
d_{46}	1.65 1.64	1.647	1.653	1.690	1.664
(001)(2 × 1)					
E_{surf}	2.12	1.99	2.14	2.61	2.60
d_{12}	1.37	1.444	1.443	1.546	1.555
d_{13}	1.50	1.519	1.556	1.539	1.521
d_{34}	1.57	1.621	1.602	1.605	1.606
d_{35}	1.55	1.541	1.555	1.549	1.543

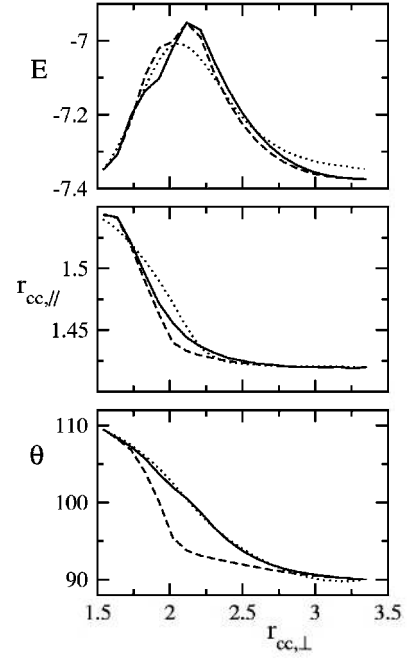


FIG. 9. The reaction path of the bulk diamond to graphite transformation as a function of $r_{CC,\perp}$ (in Å), the carbon-carbon distance perpendicular to the (111) bilayers that transform into graphitic layers, compared with the *ab initio* results from Ref. 37. The path is characterized by: the energy barrier E (in eV) (top panel), the intraplanar carbon-carbon distance, $r_{CC,\parallel}$ (in Å) (middle panel), and the buckling angle θ (in degrees) (bottom panel). Solid line: LCBOPH; dashed line: LCBOPH⁺; dotted line: Ref. 37.

the reaction path are much better reproduced by LCBOPH. The agreement with the *ab initio* results is perfectly satisfactory.

D. Vacancy in diamond and graphite

We have calculated by DF the energy of formation of a vacancy in diamond, $E_{vac}^d = 5.64$ eV and in a single layer of graphite $E_{vac}^{gr} = 7.90$ eV to determine the values of the parameters $F_{23,1}^{conj} = F_{32,1}^{conj}$ and $F_{21,0}^{conj} = F_{12,0}^{conj}$, respectively. Previous DF calculations gave $E_{vac}^d = 7.2$ eV (Ref. 38) and $E_{vac}^{gr} = 7.6$ eV.³⁹ LCBOPH gives $E_{vac}^d = 6.78$ eV and $E_{vac}^{gr} = 7.90$ eV. For both graphite and diamond, according to our DF calculations the first neighbors move away radially from the vacancy up to a distance of 1.52 and 1.73 Å, to be compared to LCBOPH values 1.44 and 1.67 Å, for graphite and diamond, respectively. The distance between first and second neighbors of the vacancy is 1.40 Å for graphite and 1.50 Å for diamond, in good agreement with our DF data of 1.40 and 1.49 Å, respectively.

E. The 5-77-5 defect of graphite

The energetics of defect formation is very relevant for understanding diffusion and growth. An important defect in graphite is the so-called 5-77-5 topological defect shown in Fig. 10 which is formed by rotating a carbon-carbon bond by $\pi/2$ within a graphitic sheet, implying a transformation of

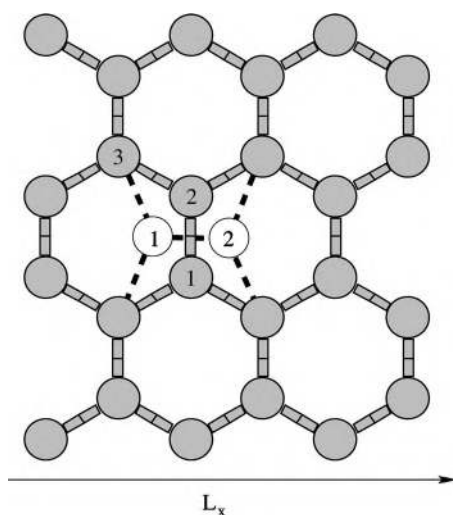


FIG. 10. Illustration of the formation of the 5-77-5 defects in graphite in a roughly square sample with side L_x . We show how the defect is formed by rotation of $\pi/2$ of the bond between atoms 1 and 2, transforming four hexagons into two pentagons and two heptagons, hence the 5-77-5 name of the defect. A rotation of the bond between atoms 2 and 3 gives an equivalent transformation.

four hexagons into two pentagons and two heptagons. This rotation is also called a Stone-Wales transformation⁴⁰ and plays an important role in the formation of fullerenes and nanotubes. A tight-binding calculation by Pan *et al.*⁴¹ for this defect resulted in a formation energy of 4.43 eV, a value much lower than the 10.4 eV previously found by Kaxiras and Pandey by means of *ab initio* calculations.³⁹ The discrepancy is attributed by Pan *et al.* to a too small sample of 18-atoms used in Ref. 39, making unreliable also the activation barrier of 13.7 eV calculated in this paper. In Fig. 11 we show the prediction of LCBOPII for these quantities that indeed confirm that formation and activation energy of this defect markedly depends on the sample size and shape. Notice that the defect can be obtained in two equivalent ways, by rotating the bond between atoms indicated as 1 and 2 or that between atoms indicated as 2 and 3 in Fig. 10. However, the calculated energies become equal only in the limit of large samples. In the bottom panel of Fig. 11 we give the values of barrier height and formation energy of this defect calculated for rotation of the 1–2 and 2–3 bonds as a function of the side L_x of the, periodically repeated, samples as shown in Fig. 10. One can see that the results for these two cases converge only for very large sizes.

For the largest sample we show in the top panel of Fig. 11 the calculated energy as a function of the rotation angle ϕ for three cases, for graphene, i.e., a single layer of graphite, for a single layer of graphite with positions constrained into the graphite plane, and for bulk graphite. As expected the last two cases are almost undistinguishable and at slightly higher energy than for graphene with out-of-plane relaxation.

IV. CONCLUSIONS

We have presented LCBOPII, an improved long-range reactive bond-order potential for carbon with the long-range

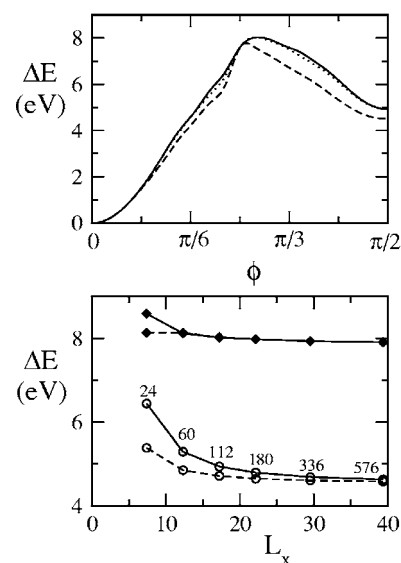


FIG. 11. Bottom panel: barrier height (filled diamond) and formation energy (empty circles) of the 5-77-5 defect calculated for rotation of the 1–2 (solid line) and 2–3 (dashed line) bonds as a function of the side L_x of the samples defined in Fig. 10. As indicated, the total number of atoms in the sample ranges between 24 and 576. One can see that the two estimates converge only for the largest sizes. For the largest sample we show in the top panel the calculated energy as a function of the rotation angle ϕ for three cases: graphene, i.e., a single layer of graphite (dashed line), graphene with positions constrained into the plane (dotted line), and bulk graphite (solid line).

interactions cutoff at 6 Å, ensuring interplanar binding in graphite. Several new concepts have been introduced in the construction of this potential to improve the reactivity and the description of the structure and energetics of all carbon phases. We have also performed DF calculations of selected structures to extend the database for fitting to relevant structures not found in the literature. In the companion paper, the description of LCBOPII for liquid carbon is shown to be extremely accurate up to extreme pressures and temperatures, confirming the high transferability and predictivity of this potential. After a complete description of LCBOPII, we have given results for the structure and energetics of bulk and surfaces, for the graphite-to-diamond transformation, and for the vacancy defect in diamond and graphite. Moreover, we give original predictions for the energetics of formation of the 5-77-5 defect of graphene and graphite. We believe that the new formulation to describe reactivity and bonding through quantities representing dangling bonds and occupied antibonding states can inspire further progress in the construction of accurate reactive potentials, also for other materials.

ACKNOWLEDGMENTS

This work is part of the research program of the “Stichting voor Fundamenteel Onderzoek der Materie (FOM),” which is financially supported by the “Nederlandse Organisatie voor Wetenschappelijk Onderzoek (NWO).” J.H.L. and

TABLE V. Parameters of the angular function [Eq. (A3)] and torsional term [Eq. (A4)] of LCBOP⁺.

$y_0 = -1/3$	
$\gamma_0 = 0.128688658$	$\gamma_1 = 0.462131068$
$T_0 = -0.182177564$	$T_1 = -0.0147711739$

A.F. acknowledge NWO Project No. 015.000.031 for financial support. E.J.M. acknowledges the Royal Netherlands Academy of Art and Sciences for financial support. We acknowledge support from the Stichting Nationale Computerfaciliteiten (NCF) and the Nederlandse Organisatie voor Wetenschappelijk Onderzoek (NWO) for the use of super-computer facilities. We thank Berend Smit for his interest in this work.

APPENDIX A: LCBOP⁺

In Refs. 23 and 25 we have used LCBOP⁺, an improvement of the potential LCBOP of Ref. 22 (called LCBOP in this paper) by (i) a modification of the switch functions, (ii) a correction of the angular function for small angles and low coordinations, and (iii) the addition of torsional interactions.

The switch function $f_{c,ij}$ in LCBOP [Eq. (1) in Ref. 22] was replaced by $S_{sr,ij}^{down}$. The switch function in the definition of the coordination [Eq. (10) in Ref. 22] was replaced by $S_{N,ij}^{down}$. Thus both these switch functions are the same as for LCBOPII.

The function $G(\cos \theta)$ of LCBOP, being fitted to solid state configurations, where low angles occur only for structures with high coordination, (e.g., simple cubic with six neighbors or fcc with 12 neighbors) was not able to stabilize small clusters, for which angles of 90° or 60° are common. The angular function of LCBOP⁺ is written in a similar form as for LCBOPII [Eq. (12)]:

$$G_{I^+}(y, z) = \Theta(y_0 - y)G_I(y) + \Theta(y - y_0)\tilde{G}_{I^+}(y, z), \quad (\text{A1})$$

where G_I is the angular function G of LCBOP, $y = \cos \theta_{ijk}$, $y_0 = -1/3$ is a constant boundary value, and $z = z_{ij} = N_i - S_{N,ij}^{down}$. The function \tilde{G}_{I^+} reads

$$\tilde{G}_{I^+}(y, z) = G_I(y) + S_{2,3,0}^{down}(z)[\Gamma(y) - G_I(y)], \quad (\text{A2})$$

where

$$\Gamma(y) = \gamma_0(y - 1)^3 + \gamma_1 \quad (\text{A3})$$

and where the subscript numbers (2,3,0) of the switch function $S_{2,3,0}^{down}$ are the upperbound, the lowerbound, and the value of p , according to the definition in Sec. II A, respectively. The parameters γ_0 and γ_1 , given in Table V, are fitted to the geometries and energies of a planar rhombic cluster (C_4 , symmetry D_{2h} , Ref. 29), with two angles around 60°, and a cubic cluster (C_8 , Ref. 30), with all 24 angles at 90°.

As for LCBOPII, the torsional term acts only for a bond between two sp_2 hybridized atoms. For LCBOP⁺ it is fitted to the data of Ref. 27, that are in agreement with our own DF results presented in Appendix B. The torsion term T_{ij} is

$$T_{ij} = D_{ij}(N_{ij}, N_{ji}) \sum_{k \neq i, j} \sum_{l \neq i, j} t_{ij}(\tilde{y}, N_{ij}^{conj}) S_{sr}^{down}(r_{ik}) S_{sr}^{down}(r_{jl}), \quad (\text{A4})$$

where \tilde{y} is defined as

$$\tilde{y} \equiv \cos \theta_{ijkl} = \mathbf{e}_{ijk} \cdot \mathbf{e}_{jil} = \frac{\mathbf{r}_{ij} \times \mathbf{r}_{ik}}{|\mathbf{r}_{ij} \times \mathbf{r}_{ik}|} \cdot \frac{\mathbf{r}_{ji} \times \mathbf{r}_{jl}}{|\mathbf{r}_{ji} \times \mathbf{r}_{jl}|}$$

and $D_{ij}(N_{ij}, N_{ji})$ is a two-dimensional switch, defined for $N_{ij}, N_{ji} \in [1, 3]$, given by

$$D_{ij}(N_{ij}, N_{ji}) = \tilde{D}(x, y) = (1 - x)^4(1 - y)^4(1 + 4x)(1 + 4y) \times \Theta(x + 1)\Theta(1 - x)\Theta(y + 1)\Theta(1 - y), \quad (\text{A5})$$

with $x = |N_{ij} - 2|$ and $y = |N_{ji} - 2|$. This definition yields $D_{ij}(2, 2) = 1.0$, $D_{ij}(n, m) = 0$ when either n or m is 1 or 3, and vanishing partial derivatives for all nine integer pairs (n, m) . In contrast to Refs. 42 and 16, where the dependence on N_{ij}^{conj} is included in the prefactor D_{ij} , for LCBOP⁺ the angle and N_{ij}^{conj} dependencies of the torsional interaction are coupled, in accordance with the DF results, and included in the function t_{ij} , which reads

$$t_{ij}(\tilde{y}, N_{ij}^{conj}) = \tau_0(\tilde{y}) + \tilde{S}(N_{ij}^{conj})[\tau_1(\tilde{y}) - \tau_0(\tilde{y})], \quad (\text{A6})$$

where

$$\tau_0(\tilde{y}) = T_0(\tilde{y}^2(1 - \tilde{y}^2))^2, \quad (\text{A7})$$

$$\tau_1(\tilde{y}) = T_1(1 - \tilde{y}^2)(2 - \tilde{y}^2)^2 \quad (\text{A8})$$

describe the torsional barriers for $N_{ij}^{conj} = 0$ (Fig. 5), and $N_{ij}^{conj} = 1$ (Fig. 5), respectively, and where the switch function $\tilde{S}(N_{ij}^{conj})$ given by

$$\tilde{S}(N_{ij}^{conj}) = [3(N_{ij}^{conj})^2 - 2(N_{ij}^{conj})^3]^2 \quad (\text{A9})$$

quickly decays from $N_{ij}^{conj} = 1.0$, in order to associate the maximal barrier only to configurations close to the double bonded ones. The values for T_0 and T_1 are given in Table V.

APPENDIX B: DETAILS OF DF CALCULATIONS

The functions t_{ij} [Eq. (35)] and V_{ij}^{mr} [Eq. (44)] are fitted to *ab initio* DF results calculated to this purpose by means of the CPMD package.⁴³ We used the spin polarized local density functional with BP^{44,45} gradient correction. The Kohn-Sham states were expanded in a plane-wave basis set sampled at the Γ point in the Brillouin zone, and truncated at a kinetic energy of 90 Ry. Semilocal norm-conserving Martins-Troullier pseudopotentials⁴⁶ were used to restrict the number of electronic states to those of the valence electrons. The pseudopotential was constructed with a valence-electron configuration s^2p^2 , using core-radii of 1.23 a.u. for both s and p orbitals. The pseudopotential was transformed into the Kleinman-Bylander form⁴⁷ with p orbitals as the local term. All calculations were performed using an isolated cubic cell.

1. Torsional barriers

In the spirit of Refs. 27 and 48, we calculated by DF the torsional barriers for the bond between the two threefold co-

ordinated atoms i and j (shaded circles in Fig. 5) for threefold (white circles) or fourfold (black circles) coordination of the other neighbors. The number N^{conj} increases with the number of fourfold sp^3 neighbors. The cases with $N^{conj}=0$ (i.e., with a conjugated π_z orbital) and $N^{conj}=1$ (i.e., the double bond) correspond to the two molecules studied in Ref. 27. Hydrogen atoms were used to obtain the correct coordination of the four peripheral atoms.

After geometrical optimization of the planar configuration, we twisted the molecule around the axis through i and j , in steps of $\pi/12$; at each step we optimized the electronic wave function without allowing any structural relaxation, in order to have the energy barrier as a function of the twisting angle only. The results, shown by symbols in Fig. 6, were used to fit the parameters of t_{ij} for LCBOPII. Note that for LCBOPII only the coordination of the peripheral atoms, and not the actual positions of the further neighbors not shown in Fig. 5, is relevant for the energy of the bond ij .

2. Dissociation energy curves

The DF dissociation energy curves for a single, double, and a triple bond, used to fit the parameters A_1^{mr} and A_2^{mr} of the middle-range potential [Eq. (50)], were calculated for three model molecules, namely $(\text{CH}_3)_3\text{C}-\text{C}(\text{CH}_3)_3$, $(\text{CH}_3)_2\text{C}=\text{C}(\text{CH}_3)_2$, and $(\text{CH}_3)\text{C}\equiv\text{C}(\text{CH}_3)$, respectively. After geometrical optimization of the molecules, the central CC-bond was stretched in steps of 0.1 Å and the wave function was optimized without allowing any relaxation. The dissociation energy was defined as the difference between twice the Kohn-Sham energy of one isolated fragment after complete dissociation and the Kohn-Sham energy of the mol-

ecule in its equilibrium geometry. The bonding energy has the opposite sign.

The dissociation energy curves according to LCBOPII were calculated using appropriate atomic configurations. For example, for the double bond we considered the stretching of the central ij bond in the configuration with $N_{ij}^{conj}=1$ in Fig. 5. In both the DF and the LCBOPII description the zero of energy was assigned to the configuration with completely dissociated fragments. The parameters A_1^{mr} and A_2^{mr} for the single and the double bond, respectively, were fitted by matching the energies at a stretching distance equal to 2.2 Å. The triple bond dissociation energy curve is already fairly well described by the potential $V^{lr}(r)$, and no middle-range interaction is added in this case.

The dissociation curves calculated by DF are reliable when the bond lengths are not too far from their equilibrium value, as well as for the dissociated fragments. However, between 2.2 Å and complete dissociation, the DF results are not *a priori* reliable, particularly when the two dissociated fragments contain unpaired spins. Therefore, consistently with Ref. 49, we assumed that there is no barrier in the formation of the single bond and monotonously connected the curve to zero for $r > 6$ Å. For the double bond, in which case the fragments do not contain unpaired spins, we found a small barrier at 2.9 Å if the molecule was kept in the planar configuration. Allowing relaxation during the dissociation, the molecule found a dissociation path without any barrier, evolving to a chair configuration from bond length 2.2 Å on. The middle-range potential for the double dangling bond cannot account for this steric difference. Therefore we did not fit the dissociation barrier for this case. The smaller barrier, shown in Fig. 8, is due to $V^{lr}(r)$.

¹S. Mayo, B. Olafson, and W. A. Goddard III, J. Chem. Phys. **94**, 8897 (1990).

²M. Finnis and J. Sinclair, Philos. Mag. A **50**, 45 (1984).

³M. I. Baskes, Phys. Rev. Lett. **59**, 2666 (1987).

⁴J. Cai and J. S. Wang, Phys. Rev. B **64**, 035402 (2001).

⁵F. H. Stillinger and T. A. Weber, Phys. Rev. B **31**, 5262 (1985).

⁶M. Z. Bazant, E. Kaxiras, and J. F. Justo, Phys. Rev. B **56**, 8542 (1997).

⁷J. F. Justo, M. Z. Bazant, E. Kaxiras, V. V. Bulatov, and S. Yip, Phys. Rev. B **58**, 2539 (1998).

⁸N. A. Marks, Phys. Rev. B **63**, 035401 (2001).

⁹J. Tersoff, Phys. Rev. Lett. **56**, 632 (1986).

¹⁰J. Tersoff, Phys. Rev. B **37**, 6991 (1988).

¹¹J. Tersoff, Phys. Rev. B **38**, 9902 (1988).

¹²J. Tersoff, Phys. Rev. Lett. **61**, 2879 (1988).

¹³A. C. T. van Duin, S. Dasgupta, F. Lorant, and W. A. Goddard III, J. Phys. Chem. A **105**, 9396 (2001).

¹⁴A. C. T. van Duin, A. Strachan, S. Stewman, Q. Zhang, X. Xu, and W. A. Goddard III, J. Phys. Chem. A **107**, 3803 (2003).

¹⁵D. W. Brenner, Phys. Rev. B **42**, 9458(E) (1990); **46**, 1948 (1992).

¹⁶D. W. Brenner, O. A. Shenderova, J. A. Harrison, S. J. Stuart, B. Ni, and S. B. Sinnott, J. Phys.: Condens. Matter **14**, 783 (2002).

¹⁷S. B. Sinnott, O. A. Shenderova, C. T. White, and D. W. Brenner, Carbon **36**, 1 (1998).

¹⁸A. Petukhov and A. Fasolino, in *Technical Proceedings of the ICCN 2001 Int. Conf. on Computational Nanoscience* (Applied Computational Research Society, Boston, 2001) p. 180, also at <http://www.nsti.org/procs/ICCN2001/6/T23.3>

¹⁹J. Che, T. Cagin, and W. A. Goddard III, Theor. Chem. Acc. **102**, 346 (1999).

²⁰S. J. Stuart, A. B. Tutein, and J. A. Harrison, J. Chem. Phys. **114**, 6472 (2000).

²¹J. Los and A. Fasolino, Comput. Phys. Commun. **147**, 178 (2002).

²²J. H. Los and A. Fasolino, Phys. Rev. B **68**, 024107 (2003).

²³L. M. Ghiringhelli, J. H. Los, E. J. Meijer, A. Fasolino, and D. Frenkel, Phys. Rev. B **69**, 100101(R) (2004).

²⁴J. N. Glosli and F. H. Ree, Phys. Rev. Lett. **82**, 4659 (1999).

²⁵L. M. Ghiringhelli, J. H. Los, E. J. Meijer, A. Fasolino, and D. Frenkel, Phys. Rev. Lett. **94**, 145701 (2005).

²⁶R. Car and M. Parrinello, Phys. Rev. Lett. **55**, 2471 (1985).

²⁷C. J. Wu, J. N. Glosli, G. Galli, and F. H. Ree, Phys. Rev. Lett. **89**, 135701 (2002).

²⁸L. M. Ghiringhelli, J. H. Los, E. J. Meijer, and A. Fasolino, Phys. Rev. B **72**, 214103 (2005).

- ²⁹K. Raghavachari and J. S. Binkley, J. Chem. Phys. **87**, 2191 (1987).
- ³⁰K. Kobayashi, N. Kurita, H. Kumahora, and K. Tago, Phys. Rev. B **45**, 11299 (1992).
- ³¹W. W. R. Nicklow and H. G. Smith, Phys. Rev. B **5**, 4951 (1972).
- ³²S. Kabalkina and L. Vereschagin, Dokl. Akad. Nauk SSSR **131**, 300 (1960).
- ³³M. T. Yin and M. L. Cohen, Phys. Rev. Lett. **50**, 2006 (1983).
- ³⁴M. T. Yin and M. L. Cohen, Phys. Rev. B **29**, 6996 (1984).
- ³⁵*Numerical Data and Functional Relationships in Science and Technology*, edited by O. Madelung, M. Schulz, and H. Weiss, Landolt-Börnstein, Vol. 17, Subvol. a: Semiconductors: Physics of Group IV Elements and III-V Compounds (Springer-Verlag, Berlin, 1982).
- ³⁶A. R. A. Aziz and H. Rafizadeh, Phys. Rev. B **7**, 4527 (1973).
- ³⁷S. Fahy, S. G. Louie, and M. L. Cohen, Phys. Rev. B **34**, 1191 (1986).
- ³⁸J. Bernholc, A. Antonelli, T. M. Del Sole, Y. Bar-Yam, and S. T. Pantelides, Phys. Rev. Lett. **61**, 2689 (1988).
- ³⁹E. Kaxiras and K. C. Pandey, Phys. Rev. Lett. **61**, 2693 (1988).
- ⁴⁰A. J. Stone and D. J. Wales, Chem. Phys. Lett. **128**, 501 (1986).
- ⁴¹B. C. Pan, W. S. Yang, and J. Yang, Phys. Rev. B **62**, 12652 (2000).
- ⁴²D. W. Brenner, J. H. Harrison, C. T. White, and R. J. Colton, Thin Solid Films **206**, 220 (1991).
- ⁴³CPMD, version 3.3, developed by J. Hutter, A. Alavi, T. Deutsch, M. Bernasconi, S. Goedecker, D. Marx, M. Tuckerman, and M. Parrinello, MPI für Festkörperforschung and IBM Zurich Research Laboratory, 1995–1999.
- ⁴⁴A. D. Becke, Phys. Rev. A **38**, 3098 (1988).
- ⁴⁵J. P. Perdew, Phys. Rev. B **33**, 8822 (1986); **34**, 7406(E) (1986).
- ⁴⁶N. Troullier and J. L. Martins, Phys. Rev. B **43**, 1993 (1991).
- ⁴⁷L. Kleinman and D. M. Bylander, Phys. Rev. Lett. **48**, 1425 (1982).
- ⁴⁸O. Kum, F. H. Ree, S. J. Stuart, and C. J. Wu, J. Chem. Phys. **119**, 6053 (2003).
- ⁴⁹F. Lorant, F. Behar, W. A. Goddard III, and Y. C. Tang, J. Phys. Chem. A **105**, 7896 (2001).